Numerical modelization of contact angle hysteresis of falling droplet under enhanced lubrication approximation

Numerical modelization of contact angle hysteresis of falling droplet under enhanced lubrication approximation

Nicola Suzzi[1] **and Giulio Croce**[1]

[1]DPIA - Dipartimento Politecnico di Ingegneria e Architettura - Universitá di Udine - Via delle Scienze - 33100 - Udine (UD) - Italy

E-mail: nicola.suzzi@uniud.it, giulio.croce@uniud.it

Abstract. Moving contact lines are involved in several engineering applications: in in-flight icing phenomenon, the eventual transition from droplet to rivulet or continuous film regime is crucial for the prediction of ice accretion over the aircraft surface; absorption process through structured packing is also characterized by a thin film flowing over the corrugated sheets. Disjoining pressure together with the assumption of a thin precursor film is largely used in numerical simulations of thin films and moving droplets in order to model the dynamics of moving contact lines and the surface wettability properties, in terms of imposed static contact angle. The disjoining pressure model was largely validated in case of falling films with the well known Voinov-Hoffman-Tanner law. On the other side, the capability of the disjoining pressure to model the contact angle hysteresis, which is a crucial parameter for predicting moving droplets behavior, has not been discussed yet. Here, numerical simulations of both falling films and moving droplets under lubrication approximation are conducted and the disjoining pressure model is used to predict the contact line dynamics. After verification of the full curvature implementation for a 1D falling film, the effective contact angle hysteresis is estimated for a moving droplet under different flow conditions and the transition from droplet to rivulet regime detected.

1. Introduction

The hydrodynamics of moving wetting lines still represents a complex phenomenon, characterized by physical discontinuities and different flow regimes. Indeed a thin liquid layer may evolve as a continuous film, an ensemble of rivulets, a droplet population or a combination of the mentioned regimes, with the occurrence of instability phenomena leading to a sudden change in the liquid layer configuration. Indeed, finger instability and moving dry patches have been largely analyzed in the Literature experimentally [1, 2] and, under the assumption of lubrication theory, both numerically and analytically [3–7]. Lubrication approximation, which allows to investigate hydrophilic surfaces, characterized by static contact angle $\theta_s < 90°$, has the advantage to reduce the physical 3D problem to a 2D mathematical problem, ensuring a consistent reduction in computational cost when numerical computations are required. However, the numerical studies are mainly limited to even lower values of the static contact angle, with $\theta_s < 30°$ usually investigated, due to the small slope approximation. Furthermore, the disjoining pressure model, usually adopted to model the contact line singularity, has been validated in the framework of moving film front, while, excluding the precursor work of Schwartz and Eley [8], its capability to properly model the droplet dynamics and the receding contact lines has not been tested yet. On the other side, the evolution of a liquid layer over a solid surface is involved in a number of engineering applications, such as in-flight icing on the aircraft surface, where the ice accretion is driven by the evolution of a droplet population [9], or absorption/distillation processes

through structured packing [10, 11].
Here the governing lubrication equations are numerically solved using an in-house code, previously developed and validated by the Authors [10, 12]. The small slope approximation is abandoned in favor of the full implementation of the film capillary pressure, allowing to investigate static contact angle up to $\theta_s = 60°$. Thus, the dynamics of a falling film and the occurrence of film rupture are studied, verifying consistency of the computed dynamic contact angle with the well known Hoffman-Tanner-Voinov law and discussing the benefit deriving from full curvature implementation instead of the small slope approximation. Then, a stand-alone droplet down a vertical plate is investigated and the apparent contact angle traced over the wetted perimeter. After the validation of the actual contact angle along the whole droplet with a literature, empirical correlation, the contact angle hysteresis is traced as a function of the flow characteristics, defined by the droplet Bond number, and the surface wettability, when the droplet regime is supported.

2. Mathematical model

Consider a thin liquid film flowing down a vertical plate. Applying Nusselt film theory, the undisturbed film thickness h_0 and the film velocity u_0 can be expressed as

$$u_0 = \frac{\rho\, g\, {h_0}^2}{3\,\mu}. \tag{1}$$

Lubrication theory allows to integrate continuity equation across the film thickness. Further assuming negligible film inertia, the momentum equation gives a parabolic velocity profile, which can be averaged across the film thickness and substituted in the continuity equation, leading to

$$\frac{\partial h}{\partial t} + \nabla \cdot \left(\frac{\rho\, \mathbf{g}\, h^3}{3\,\mu} - \frac{\nabla p}{3\,\mu} h^3 \right) = 0, \tag{2}$$

where h is the unknown film thickness and p is the local film pressure,

$$p = -2\,\sigma\,\kappa - \Pi, \tag{3}$$

with 2κ being the free surface curvature, required to calculate capillary pressure, and Π the disjoining pressure. The small slope approximation,

$$2\,\kappa = \nabla^2 h, \tag{4}$$

is usually adopted to estimate the free surface curvature. However, Eq. (4) is not accurate when the contact angle exceeds $\theta_s = 30°$ [13]. Following [10, 12, 14], the free surface curvature is estimated as

$$2\,\kappa \simeq \frac{\frac{\partial^2 h}{\partial x^2} + \frac{\partial^2 h}{\partial y^2}}{\left[1 + \left(\frac{\partial h}{\partial x}\right)^2 + \left(\frac{\partial h}{\partial y}\right)^2\right]^{3/2}}, \tag{5}$$

which allows to investigate contact angles up to at least $\theta_s = 60°$.
The disjoining pressure, which is related to intermolecular forces arising between solid and liquid surfaces, was integrated with lubrication theory by Schwartz and Eley [8],

$$\Pi = b \left[\left(\frac{d}{h}\right)^n - \left(\frac{d}{h}\right)^m \right] \tag{6}$$

$$b = f\, \frac{(n-1)(m-1)}{n-m}\, \frac{\sigma}{d}\, (1 - \cos\theta_s)\,, n > m > 1 \tag{7}$$

where d is the precursor film thickness and θ_s is the static contact angle. The correction coefficient f,

$$f = 1 + 6.069\,\delta + 161.7\,\delta^2 - 1547\,\delta^3 + 5890\,\delta^4 \tag{8}$$

with $\delta = d/h_0$ being the non-dimensional precursor film, was introduced by Zhao and Marshall [3], in order to extend disjoining pressure to non-infinitesimal values of the precursor film thickness, as it usually happens in numerical simulation.
Introducing the following non-dimensional quantities,

$$H = \frac{h}{h_0}, \mathbf{X} = \frac{\mathbf{x}}{l_0}, T = \frac{t}{(u_0/l_0)}, \Pi^* = \frac{1}{1-\cos\theta_s}\frac{\Pi}{(\sigma/h_0)}, \Gamma = \frac{1-\cos\theta_s}{Bo^{2/3}} \tag{9}$$

with Bo and l_0 being the film Bond number and the characteristic length scale [3] respectively,

$$Bo = \frac{\rho\, g\, {h_0}^2}{\sigma}, l_0 = \left(\frac{\sigma\, h_0}{\rho\, g}\right)^{1/3}, \tag{10}$$

the governing lubrication equations, Eqs. (2), (3) and (5) can be recast as

$$\frac{\partial H}{\partial T} + \nabla\cdot\left(H^3 - \nabla P H^3\right) = 0 \tag{11}$$

$$P = -2K - \Gamma\Pi^* \tag{12}$$

$$2K \simeq \frac{\frac{\partial^2 H}{\partial X^2} + \frac{\partial^2 H}{\partial Y^2}}{\left[1 + Bo^{2/3}\left(\frac{\partial H}{\partial X}\right)^2 + Bo^{2/3}\left(\frac{\partial H}{\partial Y}\right)^2\right]^{3/2}}. \tag{13}$$

Eqs. (11), (12) and (13) are numerically solved on a structured computational grid. To do so, an in-house Finite Volume Method (FVM) solver, developed in `FORTRAN`, parallelized through `OpenMP` library for a shared memory machine and previously validated by the Authors [10,12,14] for contact angles up to 60°, is used. The Alternating Direction Implicit (ADI) method proposed by [15] is implemented for marching in time.

3. Problem statement

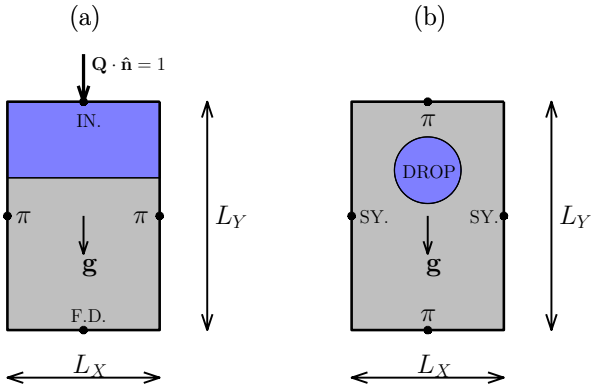

Figure 1. Investigated test cases and imposed boundary conditions (π – periodic; SY. – symmetry; IN. – inlet; F.D. – fully developed): 1D falling film (a); 2D stand-alone, moving droplet (b).

Two different test cases are investigated:

1. First, a 1D film falling down a vertical plate is investigated, Figure 1(a). Thus, periodic conditions are applied through the lateral boundaries, $X = 0$ and $X = L_X$ (giving an infinitely wide plate), while the liquid is uniformly injected through the inlet section, located at $Y = 0$, where $\mathbf{Q} \cdot \hat{\mathbf{n}} = 1$ and $H = 1$ are implemented, with $\mathbf{Q}$ being the non-dimensional film flux,

$$\mathbf{Q} = H^3 - \nabla P H^3. \tag{14}$$

Fully developed flow condition, $\nabla P \cdot \hat{\mathbf{n}} = 0$ and $\nabla H \cdot \hat{\mathbf{n}} = 0$, is imposed through $Y = L_Y$. The vertical plate is initialized with the precursor film thickness, $H|_{T_0} = \delta$. Simulations are conducted computing the free surface curvature using both the small slope approximation, Eq. (4), and the full expression provided by Eq. (13), which gives the exact curvature in case of a 1D film. The computational domain dimensions are set to $L_X = 1, L_Y = 50$ in order to ensure that the moving liquid front becomes self similar before reaching the bottomest plate section.

2. Then, a 2D droplet over a vertical plate of dimension $L_X \times L_Y$ is investigated, Figure 1(b). Periodic conditions are imposed through both the topmost section, $Y = 0$, and the bottomest section, $Y = L_Y$, giving an infinitely long plate, while symmetry condition, $\mathrm{Q} \cdot \hat{\mathbf{n}} = 0$ and $\nabla h \cdot \hat{\mathbf{n}} = 0$, is imposed at the lateral boundaries, $X = 0$ and $X = L_X$. The droplet is initialized as a spherical cap with prescribed contact angle θ_s at the center of the computational domain; the remaining initially dry region is initialized with the precursor film δ. The droplet Bond number is defined as the Bond number of the equivalent film, which is in turn defined by the average liquid thickness covering the spherical cap base area. Thus, the equivalent film thickness h_0 can be reduced to the radius r_0 of the initialized spherical cap,

$$\frac{h_0}{r_0} = \frac{(1 - \cos\theta_s)(2 + \cos\theta_s)}{3\,(1 + \cos\theta_s)}. \tag{15}$$

The free surface curvature is estimated through Eq. (13), allowing to simulate contact angles up to 60°.

4. Result

First of all, a film falling over a vertical plate (test case 1.) is investigated. Parametric computations are run and the dynamic contact angle, which is estimated from the maximum value of the film slope over the apparent contact line, traced as a function of the Bond number and the surface wettability, defined by the imposed static contact angle. Furthermore, the critical Bond number, leading to film instability, is also traced at different surface wettabilities. The spatial discretization step is set to $\Delta X = \delta/2$, in order to ensure grid independency, while the precursor film thickness and the disjoining pressure coefficients are set to $\delta = 5 \times 10^{-2}$ and $n = 3, m = 2$, according to Literature suggestions [3, 8, 16].

It is important to point out that, when small slope approximation is assumed, such a restrictive case (gravity driven film down a vertical plate) allows to reduce the two non-dimensional input parameters, *Bo* and θ_s, in a single parameter Γ, defined in Eq. (9), meaning that a single computation can be extended to a family of solutions in terms of *Bo* and θ_s. In fact, once the critical condition leading to film rupture is detected, it can be extended to any surface wettability. However, this is no more valid if the exact free surface curvature is computed via Eq. (13). The 1D computations are run both assuming small slope approximation and using the full curvature model, Eq. (13).

As a prove, the free surface profiles of the stable film solution and of the self similar droplet, the latter generated due to film rupture, are shown in Figures 2(a) and 2(c) at 3 different values of the static contact angle, $\theta_s = 30^\circ, 45^\circ, 60^\circ$, but the same Γ (with $\Gamma = 3.36$ leading to a stable film and $\Gamma = 3.92$ leading to film rupture), showing that different free surface profiles are obtained. Indeed, higher slopes are predicted at increasing θ_s, for both the stable film and the self similar droplet. The small slope approximation would hide this effect, leading to a single solution for both the stable film and the self similar droplet: Figures 2(b) and 2(d) demonstrates that the interface solution, obtained via full curvature modelization, progressively diverges from the one obtained assuming small slope approximation as $\theta_s > 30^\circ$.

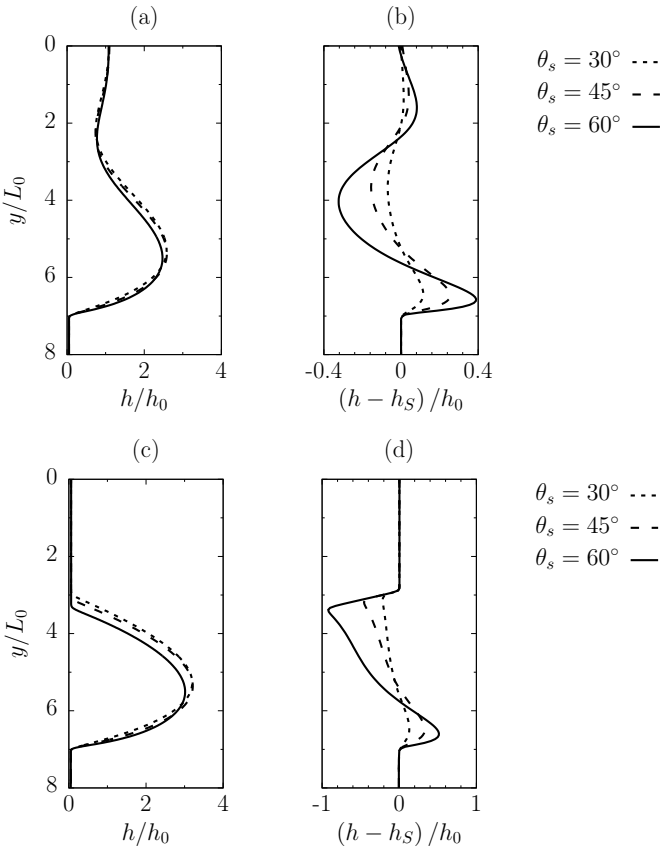

Figure 2. Self similar solutions of a 1D film falling over a vertical plate at different surface wettabilities ($\theta_s = 30°, 45°, 60°$): stable film at $\Gamma = 3.36$ (a); difference between small slope solution, h_S, and full curvature implementation at $\Gamma = 3.36$ (b); droplet generated due to film rupture at $\Gamma = 3.92$ (c); difference between small slope solution, h_S, and full curvature implementation at $\Gamma = 3.92$. Test case 1.

The dynamic contact angle in the stable film range is shown in Figure 3 as a function of the Bond number. Numerical results are consistent with the modified Hoffman-Voinov-Tanner law [17],

$$\left(\frac{\theta}{\theta_s}\right)^3 = C + Bo\left[D + E\log\left(Bo^{1/3}\right)\right] \tag{16}$$

with C being a constant coefficient introduced by Zhao and Marshall [3], D and E being constant coefficients as well. Furthermore, the dynamic contact angle always collapse to the corresponding static contact angle at Bond number approaching zero (i.e. static contact line).
The dashed line in Figure 3, which refers to small slope approximation, is obtained by reducing the detected dynamic contact angle of the continuous film at incipient film instability. It is worth to point out that the small slope approximation is not able to accurately predict the actual contact angle even at $\theta < 30°$. However, the film instability occurrence (i.e. the critical Bond number) is still correctly predicted.

The 2D computations of the stand-alone droplet (test case 2.) are run imposing spatial discretization step equal to $\Delta X, \Delta Y \leq 2/3\,\delta$, while the disjoining exponents are set again to $n = 3, m = 2$. Two different values of the precursor film thickness, $\delta = 5\times10^{-2}$ and $\delta = 2.5\times10^{-2}$, are investigated. The equivalent film thickness h_0, which defines the droplet Bond number and is required to initialize the spherical cap, is estimated via Eq. (15). Again, parametric computations are run and the contact angle hysteresis is traced as a function of the Bond number and the surface wettability. Since the disjoining pressure model

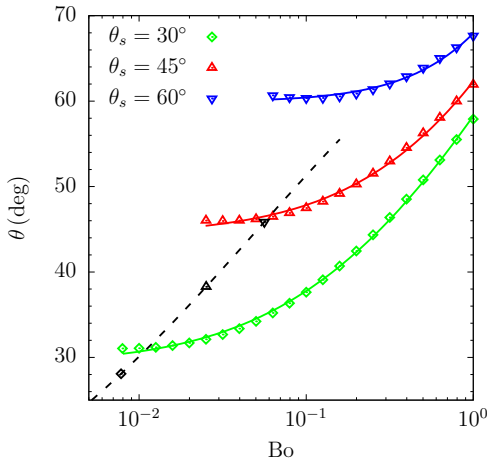

Figure 3. Dynamic (advancing) contact angle for a 1D stable film falling over a vertical plate as a function of Bond number and surface wettability: numerical results (markers) vs Eq. (16) (continuous lines). Dashed line predicts dynamic contact angle at incipient film rupture through small slope approximation. Test case 1.

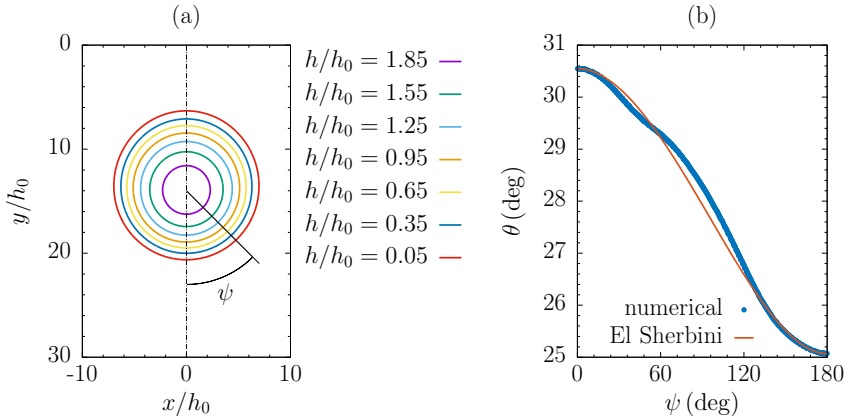

Figure 4. Self similar droplet falling down a vertical plate (a); numerical (markers) vs empirical [18] (continuous line) apparent contact angle as a function of azimuthal coordinate (b). Test case 2, $Bo = 10^{-2}$, $\theta_s = 30°$, $\delta = 5{\times}10^{-2}$.

have been largely validated and mostly used for the moving contact line of a liquid film [3, 4, 16], i.e. focusing on the advancing liquid front, a further validation is attempted in case of a falling droplet, i.e. looking at the phenomenology of a receding liquid boundary. To do so, once the slowly moving droplet becomes self similar, its apparent contact line, located where the local maximum slope is observed, is tracked over the computational domain. Thus, the droplet center of gravity is estimated and the apparent contact angle expressed as a function of the azimuthal coordinate ψ (with $\psi = 0°$ at the advancing front of the droplet and $\psi = 180°$ at the receding front). The numerical results are thus validated with the following empirical correlation [18],

$$\theta(\psi) = 2\,\frac{\cos\theta_{max} - \cos\theta_{min}}{\pi^3}\,\psi^3 - 3\,\frac{\cos\theta_{max} - \cos\theta_{min}}{\pi^2}\,\psi^2 + \cos\theta_{max}. \tag{17}$$

Figure 4(b) shows a good agreement between numerical results and empirical correlation, with a maximum uncertainty of about $\Delta/(\theta_{max} - \theta_{min}) \simeq 6\%$, meaning that we can be confident in modeling

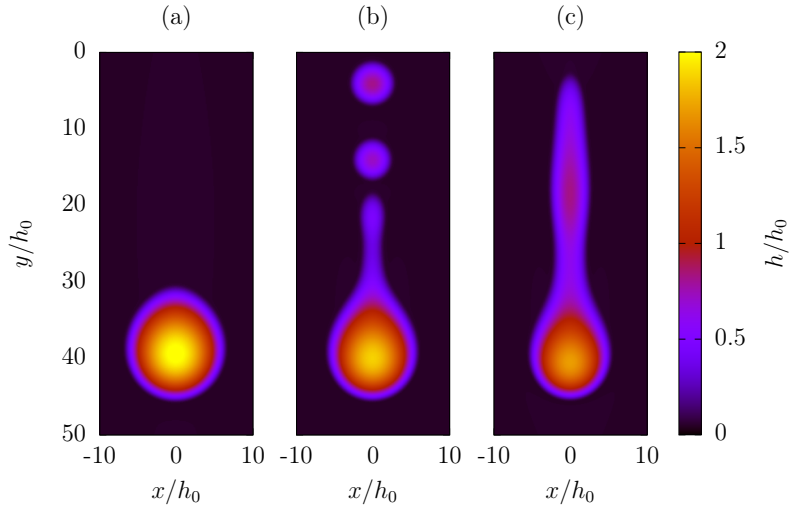

Figure 5. Liquid layer distribution at $T = 15$: $Bo = 2.00\times10^{-2}$ (a); $Bo = 3.16\times10^{-2}$ (b); $Bo = 5.01\times10^{-2}$ (c). Test case 2, $\theta_s = 30°$, $\delta = 5\times10^{-2}$.

droplet contact line dynamics along the whole droplet perimeter through disjoining pressure model. The corresponding droplet shape, shown in Figure 4(a), was obtained from a computation at relatively low Bond number, $Bo = 10^{-2}$, and $\theta_s = 30°$.

Increasing the droplet Bond number at fixed θ_s, the initial spherical cap deforms due to gravity. As

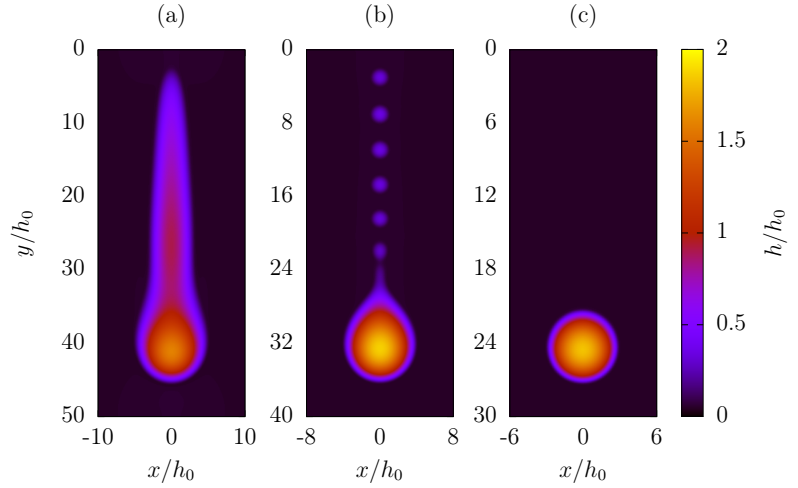

Figure 6. Liquid layer distribution at $T = 15$: $\theta_s = 30°$ (a), $\theta_s = 45°$ (b), $\theta_s = 60°$ (c). Test case 2, $Bo = 7.94\times10^{-2}$, $\delta = 5\times10^{-2}$.

shown in Figure 5, the moving, self similar droplet gets progressively stretched, until a critical condition is reached. In fact, when $Bo = 3.16\times10^{-2}$, the initial droplet breaks due to capillary instability, inducing formation of multiple droplets slowly draining down the vertical plate. Thus, a bifurcation can be observed for the droplet solution, as previously detected for the 1D falling film. Even something more similar to a long rivulet, not yet broken into smaller droplets, can be observed at higher Bond number, $Bo = 5.01\times10^{-2}$. Snapshots of Figure 5 are referred to the same non-dimensional time, $T = 15$, and the same surface wettability, $\theta_s = 30°$, but increasing Bond number.

The effect of the surface wettability is also presented in Figures 6(a), 6(b) and 6(c), which refer to the

same Bond number, $Bo = 7.94\times10^{-2}$, but different surface wettabilities. As expected, droplet regime is incentivated at lower surface wettability, with bifurcation occurring at progressively higher Bond number. It is important to point out that such a behavior of the receding contact lines was analytically reported by Eggers [19], who demonstrated through asymptotic analysis that, under lubrication approximation, the receding contact line is no more sustainable and disappears at high contact line speed, which is exactly what is here observed. This may identify the transition between droplet and rivulet regime.

The contact angle hysteresis, defined as the difference between the maximum and the minimum contact

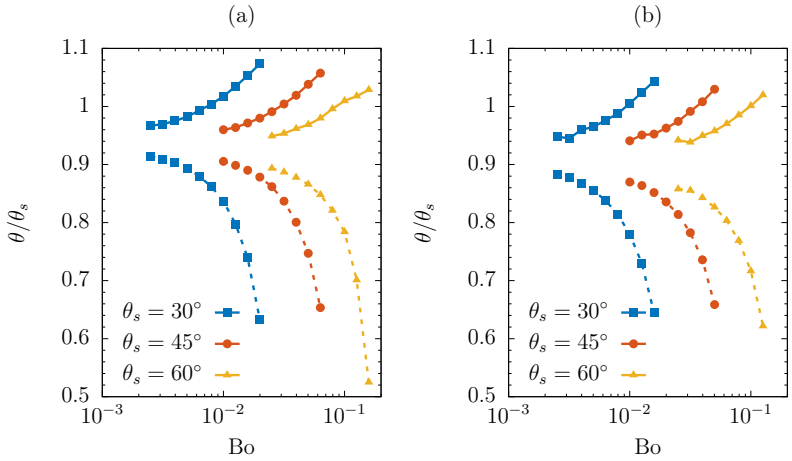

Figure 7. Normalized advancing contact angle (continuous lines) and receding contact angle (dashed lines) of a droplet down a vertical plate as a function of Bond number and surface wettability: $\delta = 5\times10^{-2}$ (a); $\delta = 2.5\times10^{-2}$ (b). Test case 2.

angle detected over the apparent contact line, is plotted in Figure 7 as a function of both the Bond number and the surface wettability. Results giving drop break up or an elongated droplet (which is more similar to a rivulet regime) are not considered since they do not provide information about the receding contact angle. Two different precursor film thickness are investigated, with Figure 7(a) referring to $\delta = 5\times10^{-2}$ and Figure 7(b) referring to $\delta = 2.5\times10^{-2}$, in order to verify its influence on the contact line dynamics. It can be observed that the contact angle hysteresis approaches zero for a sufficient low Bond number, i.e. negligible gravity forces, independently on the imposed static contact angle, meaning that the droplet progressively tends to the initialized spherical shape as its velocity tends to zero. On the other side, the contact angle hysteresis progressively increases with the Bond number and, thus, with the contact line velocity, until the critical condition leading to break up is detected. The effect of the solid surface wettability just seems to shift the hysteresis curves, with higher Bond numbers required to ensure an evident contact angle hysteresis. However, both the advancing and the receding contact angles seems to collapse to a value, which is a bit lower than the imposed static contact angle (with a discrepancy of about $\sim$5% observed for both $\delta = 5\times10^{-2}$ and $\delta = 2.5\times10^{-2}$). Such a small discrepancy is probably due to an inaccurate scaling in the definition of the Bond number, which is estimated through the equivalent film thickness, Eq. (15).

It can be also noticed that the effect of the precursor film thickness on the contact angle hysteresis is not relevant and even the critical condition (i.e. disappearance of the receding contact line) occurs at similar Bond numbers.

5. Conclusion

The governing lubrication equations were numerically solved in case of both a film down a vertical plate and a moving droplet driven by gravity. It was proved that the small slope approximation, usually adopted in literature and valid for low film slope, does not provide accurate results when $\theta_s \geq 30°$.

Indeed, computing the interface curvature via Eq. (5) ensures a proper modelization of the contact line dynamics, both for a flowing film and a moving droplet, at contact angle up to $\theta_s = 60°$. Furthermore, the disjoining pressure was validated for the first time in the framework of moving droplets, which involves a receding contact line. Indeed, the actual contact angle was traced along the whole droplet contact line and validated with a literature, empirical correlation. Thus, important information were provided about the contact angle hysteresis, which was traced as a function of the flow characteristics and the surface wettability. New instability phenomena, including droplet breakage and switch from moving droplet to rivulet regime, which are consistent with the physics of moving contact lines, were also detected. As a future work, the effect of the disjoining pressure exponents on the contact angle hysteresis should be investigated, in order to fully characterize the surface wettability properties. Furthermore, tracing the occurrence of elongated droplets or rivulets, may be crucial in the understanding the droplet behavior in practical applications as in-flight icing, which requires the definition of the threshold between droplet to rivulet regime to characterize the ice accretion model.

Nomenclature

b	disjoining coefficient
d	precursor film thickness
g	gravity acceleration
h	film thickness
H	non-dimensional film thickness
h_0	undisturbed film thickness
K	non-dimensional mean curvature
l_0	characteristic length scale
$L_{X,Y}$	non-dimensional plate size
m, n	disjoining exponents
$\hat{\mathbf{n}}$	normal outward versor
p	film pressure
P	non-dimensional film pressure
$\mathbf{Q}$	non-dimensional film flux
t	time
T	non-dimensional time
u	film velocity
u_0	undisturbed film velocity
x, y	Cartesian coordinates
X, Y	non-dimensional Cartesian coordinates
Greek symbols:	
Γ	non-dimensional disjoining coefficient
δ	non-dimensional precursor film thickness
θ	dynamic contact angle
θ_s	static contact angle
κ	mean curvature
μ	dynamic viscosity
Π	disjoining pressure
Π^*	non-dimensional disjoining pressure
ρ	density
σ	surface tension
ψ	azimuthal coordinate
Dimensionless numbers:	
$Bo = \rho g {h_0}^2/\sigma$	Bond number

References

[1] T Podgorski, J M Flesselles and L Limat 1999 *Physics of Fluids* **11** 845
[2] E Rio and L Limat 2006 *Physics of Fluids* **18** 032102
[3] Y Zhao and J S Marshall 2006 *Journal of Fluid Mechanics* **559** 355
[4] U Thiele, L Brusch, M Bestehorn and M Bar 2003 *The European Physical Journal E* **11** 255
[5] V Y Shkadov and G M Sisoev 2005 *Computers & Fluids* **34** 151
[6] J C-T Kao, A A Golovin and S H Davis 2006 *Journal of Colloid and Interface Science* **303** 532
[7] S K Wilson, B R Duffy and H Davis 2001 *European Journal of Applied Mathematics* **12** 233
[8] L W Schwartz and R R Eley 1998 *Journal of Colloid and Interface Science* **202** 173
[9] G Croce, E De Candido, W G Habashi, J Munzar, M Aube, G S Baruzzi and C Aliaga 2010 *Journal of Aircraft* **47** 1283
[10] N Suzzi and G Croce 2019 *Physics of Fluids* **31** 122106
[11] R K Singh, J E Galvin and X Sun 2016 *Chemical Engineering Science* **142** 244
[12] N Suzzi and G Croce 2017 *Journal of Physics: Conference Series* **923** 012020
[13] C A Perazzo and J Gratton 2004 *Journal of Fluid Mechanics* **507** 367
[14] N Suzzi and G Croce 2021 *Journal of Physics: Conference Series* **1868** 012010
[15] T P Witelski and M Bowen 2003 *Applied Numerical Mathematics* **45** 331
[16] M Sellier 2015 *International Journal of Multiphase Flow* **71** 66
[17] V S Ajaev 2012 *Interfacial Fluid Mechanics* (Springer)
[18] A I El Sherbini and A M Jacobi 2004 *Journal of Colloid and Interface Science* **273** 566
[19] J Eggers 2005 *Physiscs of Fluids* **17** 082106